



Isotopic dynamics of precipitation and its regional and local drivers in a plateau inland lake basin, Southwest China



Yajun Wang^a, Yu Tang^{b,c}, Yan Xu^a, Hongwei Yu^a, Xiaofeng Cao^a, Gaoqi Duan^a, Lijiao Bi^a, Jianfeng Peng^{a,*}

^a Center for Water and Ecology, School of Environment, Tsinghua University, Beijing 100084, China

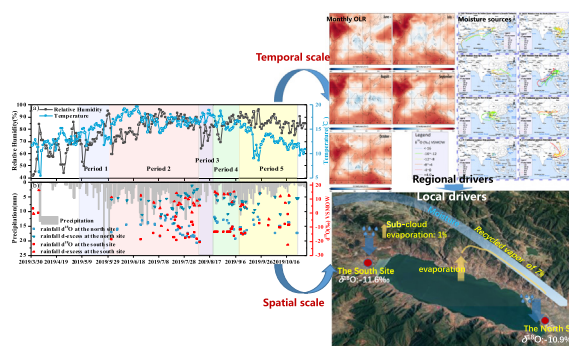
^b Natural Resources Institute Finland (LUCK), Helsinki, Finland

^c Faculty of Agriculture and Forestry, University of Helsinki, Helsinki, Finland

HIGHLIGHTS

- Convection activities and moisture sources drive the precipitation isotopic fluctuant.
- The $\delta^{18}\text{O}_p$ was negatively associated with convective activity at moisture source regions.
- Marine moisture contributed to 68% of local precipitation and the Indian Ocean contributed predominantly.
- Sub-cloud evaporation and recycled moisture explained the south-to-north rain isotope difference.

GRAPHICAL ABSTRACT



ARTICLE INFO

Article history:

Received 26 May 2020

Received in revised form 7 October 2020

Accepted 10 October 2020

Available online 16 October 2020

Editor: Christian Herrera

Keywords:

Precipitation isotopes

HYSPLIT

Meteorological factors

Convection activities

Sub-cloud evaporation

Recycled moisture

ABSTRACT

Shrinkage of plateau lakes under climate strength has drawn growing attention. Because of its intricate implication to hydro-meteorological condition and climate system, stable isotopes in precipitation (e.g. $\delta^2\text{H}_p$ and $\delta^{18}\text{O}_p$) provide us a powerful tool to understand the climate-hydrologic dynamics in shrinking lakes. However, how the regional atmospheric circulation, moisture sources and local fractionation processes drive isotopic variability from temporal to spatial scale has rarely been reported for remote plateau lakes. Hence, we collected a total of 98 rainfall samples at the south and the north shores of Chenghai lake, Yunnan-Guizhou Plateau to study the potential driving forces of precipitation isotope variability during the wet season of 2019. Based on backward trajectories of air masses obtained from HYSPLIT model, 68% of moisture came from $\delta^{18}\text{O}$ depleted ocean (Indian Ocean, Bay of Bengal, South China Sea and Pacific Ocean), and the rainout process promoted the isotopic depletion when moisture arrived at the study basin. Evapotranspiration increased the heavy isotope ratios in precipitation originated from continents (northern China inland and western continents). The temporal dynamics of $\delta^{18}\text{O}_p$ and $\delta^2\text{H}_p$ were in phase with the convection activities intensity underlined the influence from large-scale atmospheric circulation. Local meteorological factors played a secondary role in isotope variability. Precipitation amount-effect strongly affected isotope ratios while mild anti-temperature effect was observed at daily scale. Interestingly, the rainfall isotope ratios showed different mechanisms in govern at lake south shore and north shore, with a distance of 19 km in between. This south-to-north difference can be explained by either lower 1.03% sub-evaporation in the south shore or 7% of recycled moisture contributing to precipitation in the north shore. Our findings discover the driving forces for $\delta^{18}\text{O}_p$ variation and provide solid interpretations for hydro-climate change in Southwest China.

© 2020 Elsevier B.V. All rights reserved.

* Corresponding author.

E-mail address: pengjf@mail.tsinghua.edu.cn (J. Peng).

1. Introduction

Lake plays a critical role in providing water and ecosystem services for societies, especially in the plateau lake regions dominated by a hot and dry climate (Tao et al., 2020). However, plateau lakes are suffering from dramatic changes under climate change (Tao et al., 2020). Climate change influences plateau lake structure and function by direct exerting controls on hydrology, lake level, aquatic biota (Adrian et al., 2009; Cao et al., 2020; Sadro et al., 2018) and by indirect impacts on landscape changes of vegetation type and cover, tree line shift, carbon cycling and biodiversity (Gottfried et al., 2012; Harsch et al., 2009; Moser et al., 2019; Walter Anthony et al., 2018). Recent surveys suggested that 65%–75% of lake changes in Yunnan-Guizhou Plateau over the last 30 years can be explained by climate strength (Tao et al., 2020; Zhang et al., 2019). A growing attention has been drawn to the shift in climate and associated hydrological processes for the shrinking plateau lakes.

Stable isotopes in precipitation (e.g. $\delta^2\text{H}_p$ and $\delta^{18}\text{O}_p$) preserve the information of fractionation, condensation, and exchange processes along air mass pathway from its source region to the precipitation site (Dansgaard, 1964). As widely used for climate-hydrologic interpretation (Cai et al., 2019; Corcoran et al., 2019; MacDonald et al., 2016; Narancic et al., 2017), stable isotopes in precipitation can therefore help us better understanding the changing climate-hydrological processes in the plateau lakes.

Recent studies have demonstrated that the variability of precipitation stable isotopes was driven by large-scale atmospheric circulation (e.g. ENSO, ITCZ) (Cai et al., 2017, 2018; Nlend et al., 2020; Wang et al., 2020a; Wei et al., 2018). Specifically, convection activities and cloud types were considered as the dominant drivers on depleted $\delta^{18}\text{O}_p$ and $\delta^2\text{H}_p$ values at daily, seasonal and inter-annual timescale in the Asian Monsoon region (Cai et al., 2017; He et al., 2018; Nlend et al., 2020; Wang et al., 2020a). These findings were obtained by correlation analysis between local precipitation stable isotope compositions and the regional convection indexes in the upper moisture transport stream. The impact of changes in moisture sources on variations of precipitation stable isotopes was also widely discussed (e.g. Juhlke et al., 2019; Le Duy et al., 2018), by identifying moisture sources for precipitation using backward trajectory models e.g. HYSPLIT (Stein et al., 2016; Tang et al., 2017). Other processes at local scale which may change the precipitation stable isotope compositions, such as sub-cloud evaporation and recycling of continental moisture (Bowen et al., 2019; Sinha and Chakraborty, 2020; Worden et al., 2007) or mixing with other moistures (Sun et al., 2020; Wang et al., 2016) were also extensively examined.

Most studies, however, focused on either the impact of large-scale atmosphere circulation and moisture sources or the local isotopic fractionation processes. So far, limited study has yet been carried out on the combined effect of both the regional atmospheric circulation and local isotopic fractionation processes on precipitation stable isotope variability. Hence, in this paper we aimed to characterize the variability of precipitation stable isotopes with dynamics in convection activities (by the Outgoing Longwave Radiation value) and moisture sources (by HYSPLIT) as well as local meteorological conditions, in an effort to demonstrate the drivers for isotope variations at both regional and local scales.

Our study site, Chenghai Lake, is an inland plateau lake located in southwestern China. The lake level decreased from 2003 to 2016 at a rate of 3.9 m/10a, leading to an increase in salinity and changes in the presence and abundance of phytoplankton species. Chen et al. (2019) suggested that the warmer and drier climate was the main reason for the shrinkage of Chenghai Lake. The dated record of $\delta^{18}\text{O}$ in authigenic carbonates derived from lake sediments indicated that the Chenghai lake level was mainly controlled by Indian Summer Monsoon intensity (Hillman et al., 2016; Sun et al., 2019). In order to interpret the relation between the isotopic composition of rainfall and modern-day climate, we investigated the temporal and spatial variability of $\delta^{18}\text{O}_p$ and its

drive forces. The objectives of this paper were: (1) to explore the temporal dynamic of large-scale convection activities and moisture sources driving the isotopic variability in the wet season; (2) to reveal the potential mechanisms causing the spatial disparity of isotope compositions in precipitation at the north and the south shore of the lake. Our results will provide an insight to climate-hydrological processes in plateau lakes, and can serve as a valuable isotope archive for further hydrological studies.

2. Materials and methods

2.1. Study area

The Chenghai Lake basin occupying 318.3 km² (26°27'N to 26°38'N, 100°38'E to 100°41'E) is located at the middle section of Jinsha River watershed on the Yunnan-Guizhou Plateau and south of Hengduan Mountain, Southwestern China. The bowl-shaped terrain of Chenghai Lake basin involves an altitudinal gradient from mountainous peaks with a maximum height of 3275 m a.s.l., to averaged lake level of 1496 m a.s.l. (Fig. 1). Hekoujie station suited at the south shore of the lake records long-term daily values of precipitation and evaporation from water surfaces. During the past 33 years (from 1985 to 2018), annual mean precipitation was approximately 757 mm and 82% of rainfall concentrated from June to September while the annual mean water-evaporation was recorded to be 1785 mm (Fig. S1). Due to unavailability of precipitation data in 2019 from Hekoujie station, the compiled daily mean 2 m-high (above ground level, AGL) relative humidity, 2 m-high (AGL) air temperature and daily accumulated precipitation during the wet season were derived from the Global Data Assimilation System (GDAS1) (1° × 1°) archive metrological dataset (Fig. 2). No precipitation events occurred during the dry season (from November to March), thus no daily isotope values were available.

Generally, Indian Summer Monsoon was considered to be the major moisture carrier for precipitation in southwest China (Li et al., 2017b). Westerly winds prevail during April and May, while strong southwesterly winds from the Bay of Bengal and/or the Indian Ocean are the dominating moisture sources over the Yunnan-Guizhou Plateau during the wet period from June to October (Fig. S2). Where the high mountains with a peak of 3959 m a.s.l. distributed at the southwest of the study area forms a leeward region (Fig. 1). This topography combined with great evaporation from the lake might cause the difference of precipitation isotope signals at the south and the north sites when southwesterly winds blow.

2.2. Field sampling and analysis

During the observation period (April 2019 to October 2019), the daily rainfall amounts greater than 5 mm at two sites were sampled (Fig. 1). The rainfall at the north site (1512 m a.s.l.) is located about 19 km from the south site (1540 m a.s.l.). Precipitation samples were collected in pre-rinsed polyethylene bottles, tightly capped and coolly preserved until analysis in Lab. A total of 98 samples were measured for oxygen and hydrogen heavy isotope content, including 54 north samples (NS) and 44 south samples (SS).

The $\delta^{18}\text{O}_p$ and $\delta^2\text{H}_p$ compositions were determined on a liquid water isotope analyzer (LGR-DLT100, USA) at the Institute of Geographic Science and Natural Resources Research, Chinese Academy of Sciences. Results were expressed in the standard δ notation as per mil (‰) with respect to VSMOW (Vienna Standard Mean Ocean Water) standard with analytical precision of $\pm 0.1\%$ for $\delta^{18}\text{O}$ and $\pm 1\%$ for $\delta^2\text{H}$.

$$\delta = \left(\frac{R_{\text{sample}}}{R_{\text{standard}}} - 1 \right) \times 1000\text{VSMOW}$$

where R_{sample} is the $^{18}\text{O}/^{16}\text{O}$ or $^2\text{H}/^1\text{H}$ ratio of the water samples, and R_{standard} is the corresponding ratio for VSMOW. Deuterium excess (d -

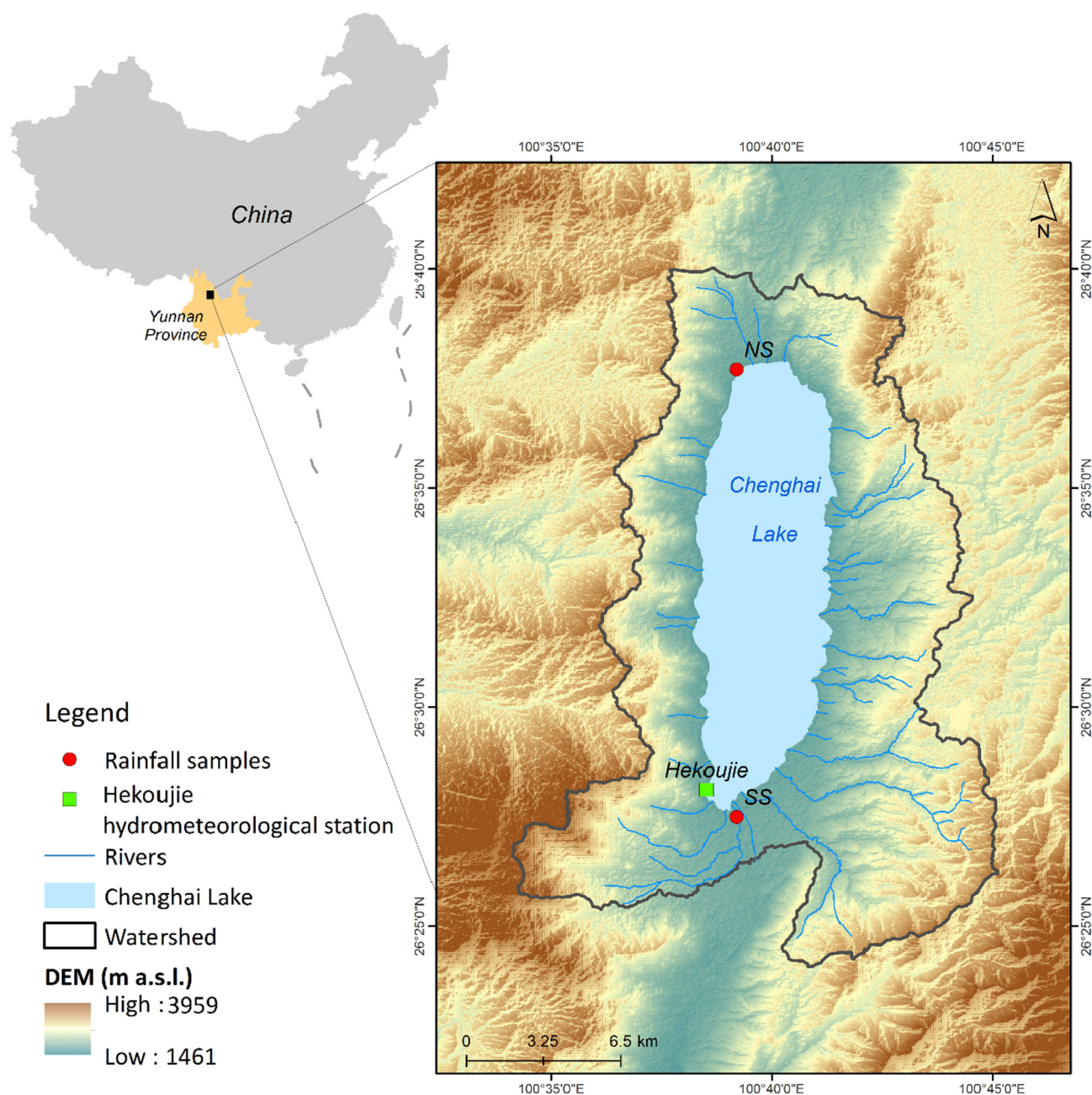


Fig. 1. Location of study area and rainfall sampling sites. NS and SS represent rainfall sampling sites located at the north shore and south shore, respectively.

excess) is calculated as $d = \delta^2\text{H} - 8\delta^{18}\text{O}$ (Dansgaard, 1964) to investigate non-equilibrium effects on the isotopic composition of precipitation, the average global d -excess of precipitation is about 10‰.

Outgoing Longwave Radiation (OLR) values less than 240 W/m^2 is indicative of large-scale organized convection (Adhikari et al., 2020). $2.5^\circ \times 2.5^\circ$ global gridded daily and monthly OLR data was downloaded from NCAR (National Center for Atmospheric Research) with temporal interpolation (https://www.esrl.noaa.gov/psd/data/gridded/data.interp_OLR.html) (Liebmann and Smith, 1996). We collected the daily (7 days before forming precipitation in the Chenghai Lake basin) and monthly OLR values at the marine areas (25.0° - 27.5° N, 100° - 102.5° E) including the India Ocean (25.0° - 27.5° N, 100° - 102.5° E), Bay of Bengal (25.0° - 27.5° N, 100° - 102.5° E) and South China Sea (25.0° - 27.5° N, 100° - 102.5° E).

2.3. Backward trajectories

To determine the origin of air masses and establish source-receptor relationships, back trajectories were performed with the hybrid single particle Lagrangian integrated trajectory (HYSPPLIT, version 4.0) air parcel tracking program in back-cast mode (<https://www.arl.noaa.gov/hysplit/hysplit/>) (Stein et al., 2016). Meteorological data from GDAS1 for the model pertained to the $1^\circ \times 1^\circ$ latitude-longitude global grid and involved an output every hour (UTC). 168-h (7 days) back trajectories were computed for the dates when precipitation was collected at the north site in the Chenghai lake basin (26.38° N, 100.39° E). We chose trajectories stimulated at the atmospheric layer of 700 hPa (3200 m) which was regarded as the maximum water vapor flux layer from June to October for the sampled precipitation.

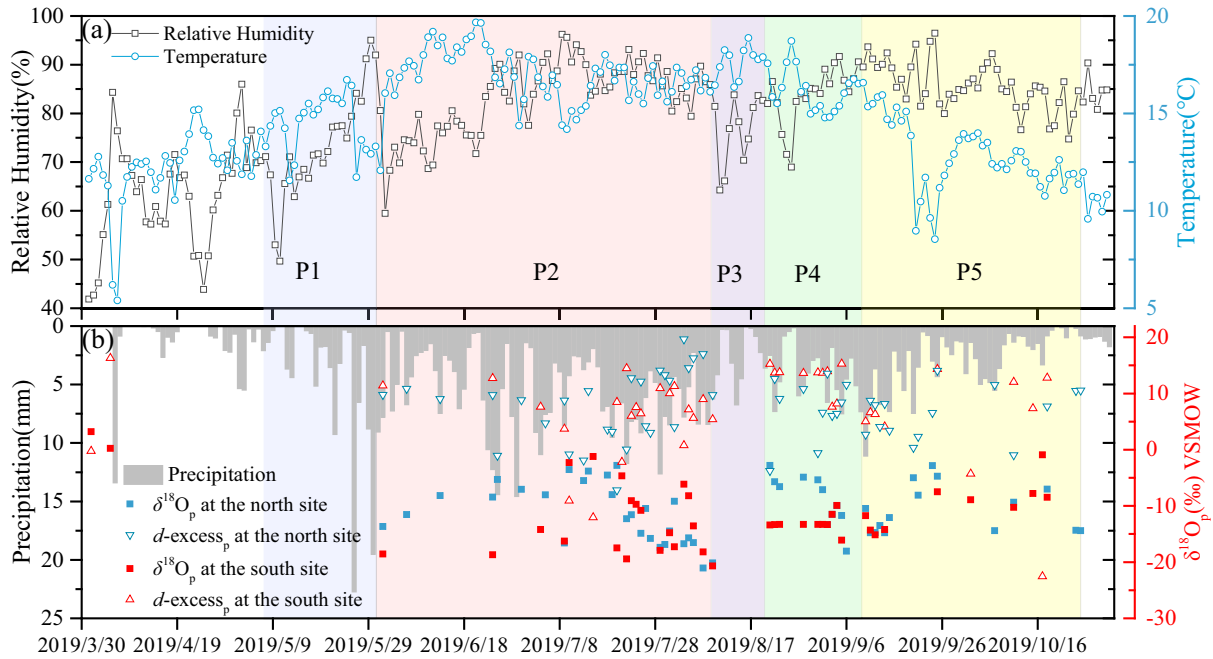


Fig. 2. Temporal characteristics of $\delta^{18}O_p$ (solid square), $d\text{-excess}_p$ (hollow triangle) and meteorological parameters, including relative humidity (black), air temperature (blue) (a) and precipitation amount (b) at 2 m above ground level in the Chenghai Lake basin. The P1- P5 periods were divided according to the variation trend of precipitation isotope values, precipitation amounts and the meteorological factors (precipitation, relative humidity and temperature).

3. Results

3.1. Isotopic ratios of rainfall and local meteoric water line

Precipitation $\delta^{18}O_p$ and δ^2H_p varied markedly from April to October 2019 (Table 1). Two samples collected on 1 April and 5 April at the south shore showed more enriched isotopic signals holding $\delta^{18}O_p$ values of 3.2‰ and 0.24‰, δ^2H_p values of 25‰ and 18‰, $d\text{-excess}_p$ values of -0.3‰ and 16.3‰, respectively. The most positive isotope values in rainwater occurred during pre-monsoon season which has also been reported in previous studies (Jiao et al., 2020; Le Duy et al., 2018). The variation of $\delta^{18}O_p$ and δ^2H_p were well synchronized in the observed period. The amount-weighted average value of $\delta^{18}O_p$ (-11.1‰) in the wet season was more positive than that at Kunming ($\delta^{18}O_p$: -11.6‰), but negative than the estimated value of -9.76‰ in Chenghai where adjacent Yongsheng County (-10.2‰) and negative than that at lower latitude regions (e.g. Mengzi (-10.8‰), Tengchong (-10.6‰)) (Hoffmann et al., 2000; Li et al., 2017a; Sun et al., 2019).

Table 1
Summary statistics of δ^2H_p , $\delta^{18}O_p$ and $d\text{-excess}_p$ of daily north rainfall samples, south rainfall samples and all rainfall samples in the Chenghai Lake basin during April to October 2019.

| Chenghai Lake Basin | | δ^2H_p (‰) | $\delta^{18}O_p$ (‰) | $d\text{-excess}_p$ (‰) |
|---------------------|------|-------------------|----------------------|-------------------------|
| NS | Max. | 21 | 0.6 | 19.7 |
| | Min. | -151 | -21.1 | -10.3 |
| | Mean | -75 | -10.3 | 1.6 |
| | Std. | 37 | 4.9 | 8.4 |
| | Max. | 25 | 3.2 | 16.3 |
| SS | Min. | -160 | -20.7 | -12.1 |
| | Mean | -86 | -11.6 | -0.1 |
| | Std. | 40 | 5.5 | 7.9 |
| | Max. | 25 | 3.2 | 19.7 |
| | Min | -160 | -21.1 | -12.1 |
| AS | Mean | -80 | -10.9 | 0.9 |
| | Std. | 39 | 5.2 | 8.2 |

The local meteoric water line (LMWL), the site-specific linear relationship between δ^2H_p and $\delta^{18}O_p$, is $\delta^2H = 7.34\delta^{18}O + 0.22$ ($R^2 = 0.98$, $n = 96$) for Chenghai Lake basin (Fig. 3), showing a significantly lower slope and intercept than the global meteoric water line (GMWL): $\delta^2H = 8\delta^{18}O + 10$ (Craig, 1961). As the southwest China belong to seasonally hot/dry regions at Köppen climate classification, sub-cloud evaporation non-equilibrium processes was probably responsible for the lower slopes of the LMWL (7.2– 7.6) than the GMWL (Putman et al., 2019). Since the sub-cloud evaporated raindrops can cause the enrichment of the heavy isotope in the remnant drop, leading to a slope < 8 of LMWL (Sinha and Chakraborty, 2020; Xu et al., 2019). This finding was further supported by a strong negative correlation between daily

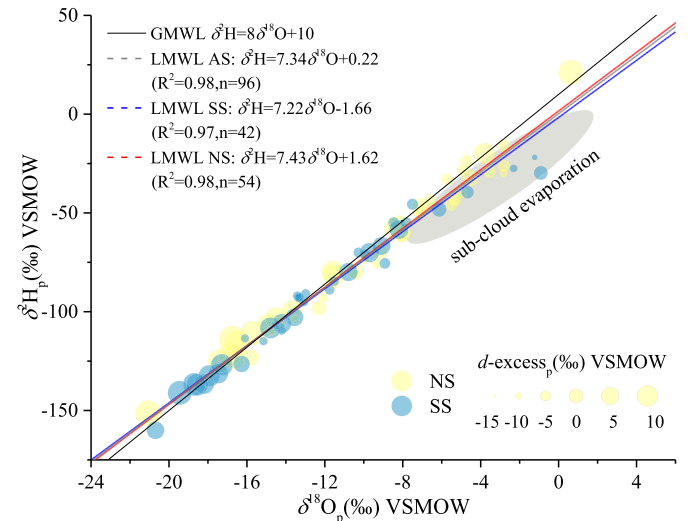


Fig. 3. The daily scattering of $\delta^{18}O_p$ and δ^2H_p in precipitation and the linear fitted local meteoric water lines (LMWLs). The bubble size represents the $d\text{-excess}$ value scale. The grey shadow ellipse region is affected by the sub-cloud evaporation, adopted from Putman et al. (2019).

$\delta^{18}\text{O}_p$ and $d\text{-excess}_p$ ($R^2 = -0.56$, $p < 0.01$, $n = 96$) (Fig. 3) (He et al., 2018).

3.2. Temporal variability of rainfall isotope

No precipitation samples were collected from early May to early June before the onset of the Summer Monsoon (Period 1, P1). P1 was marked by increasing relative humidity from 50% to 95% association with rising air temperature (from 12 °C to 16 °C) (Fig. 2). Varying $\delta^{18}\text{O}_p$ values (-21.1‰ to -1.2‰) were observed from early June to 9 August while $d\text{-excess}_p$ increased in phase (Period 2, P2). P2 corresponded to successive precipitation (amounts above 10 mm) and the higher relative humidity (60% ~ 86%) and air temperature (14 °C ~ 20 °C) attributed to the preceded monsoon activities. The precipitation amount reached its maximum (41.3 mm) on July 1, and the stable isotopes in precipitation thereafter became increasingly depleted and reached their minimum values ($\delta^{18}\text{O}_p = -21.1\text{‰}$, $\delta^2\text{H}_p = -151\text{‰}$) on August 7. During the absence of rainwater stable isotope measurement in the middle 10 days from early August to late August (Period 3, P3), the daily precipitation decreased to none or merely 8 mm, the relative humidity fluctuated between 65% and 82% and the temperature stayed at a relatively high level around 17 °C. The higher temperature and lower relative humidity might imply a higher re-evaporation and/or isotopic equilibrium of rain with ambient vapor leading to higher $\delta^{18}\text{O}_p$ in downwind precipitation at the north site in Period 4 (He et al., 2018; Le Duy et al., 2018; Xu et al., 2019). The $\delta^{18}\text{O}_p$ compositions continued to drop to values lower than -14‰ when the rainfall reached its second peak during 10 to 13 September (Period 4, P4). A slight increase $\delta^{18}\text{O}_p$ trend and reduced $d\text{-excess}_p$ was observed during 14 September to late October (Period 5, P5), accompanied by obvious decrease of rainfall, air temperature and relative humidity in response to the retreat of monsoon activity and convection southward shift. (Fig. 2). Overall, the $\delta^{18}\text{O}_p$ temporal variation showed a clear inverse pattern to precipitation amount as displayed in Fig. 2.

3.3. Spatial variability of rainfall isotope at the south and north shore

The south site and north site were marked by different precipitation stable isotope signal for different periods (Table 1 and Fig. 4). Higher average $\delta^{18}\text{O}_p$, $\delta^2\text{H}_p$ and $d\text{-excess}_p$ values were archived in NS than SS during the period P2, P4 and P1-P5, but significant only for period P4 (Anova, $p < 0.05$, Fig. 4 (d)-(f)). It appeared that the significant difference between the isotope values in the south and north precipitation was always observed before the successive rainfall events (e.g. P4 and the first half of P2).

Additionally, the slope and intercept of $\delta^2\text{H}_p\text{-}\delta^{18}\text{O}_p$ relationship were lower in SS than in NS (Fig. 3) on the southwesterly air mass transportation. This phenomenon might be associated with: 1) a large leeward region where NS collected would be in a saturation-deficit condition suitable to induce partial evaporation of raindrop leading to the enriched $\delta^{18}\text{O}_p$ in following NS rainfall (Peng et al., 2010). 2) the water vapor and rainfall isotope signals could be significantly altered by local evapotranspiration (Wei and Lee, 2019) with high coverage of forests (35%), croplands (26%) and grass lands (12%) in the watershed, and extensive lake evaporation of 1791.3 mm (Wang et al., 2020b). Evaporation of isotopically relatively uniform lake water ($\delta^{18}\text{O}_{\text{lake}} = -2.6\text{‰}$ in August) enriched the resulting water vapor in heavy isotopes might induce higher isotopic rainwater in the north site along southwesterly air transport. These processes were more noticeable during the period of P4 and the first half of P2 (Fig. 4).

3.4. Moisture sources and isotopic characteristics

Under the consideration of relative adequate rainwater collections at the north site, we chose NS to integrate the moisture sources identification with trajectory analysis in HYSPLIT. Based on the geographical position of the endpoint of back trajectories, ocean-originating (O) air parcels comprised about 68% of all trajectories, categorized into 5

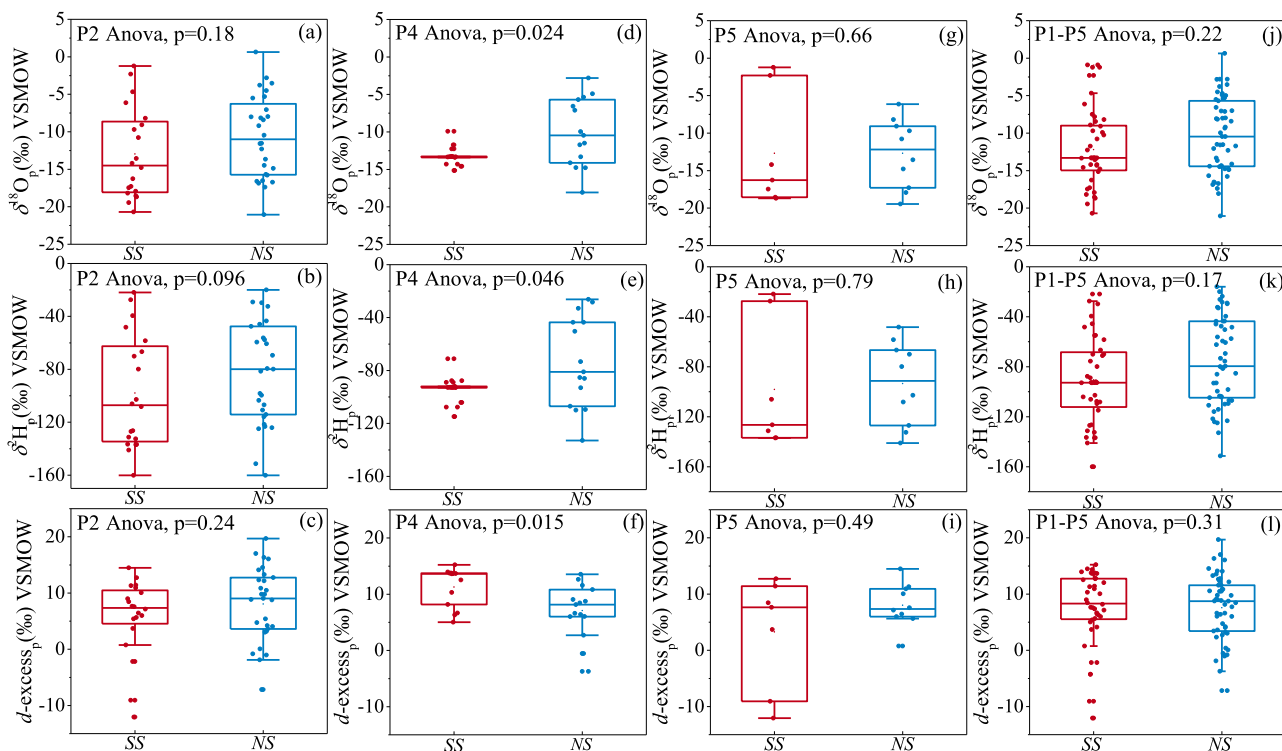
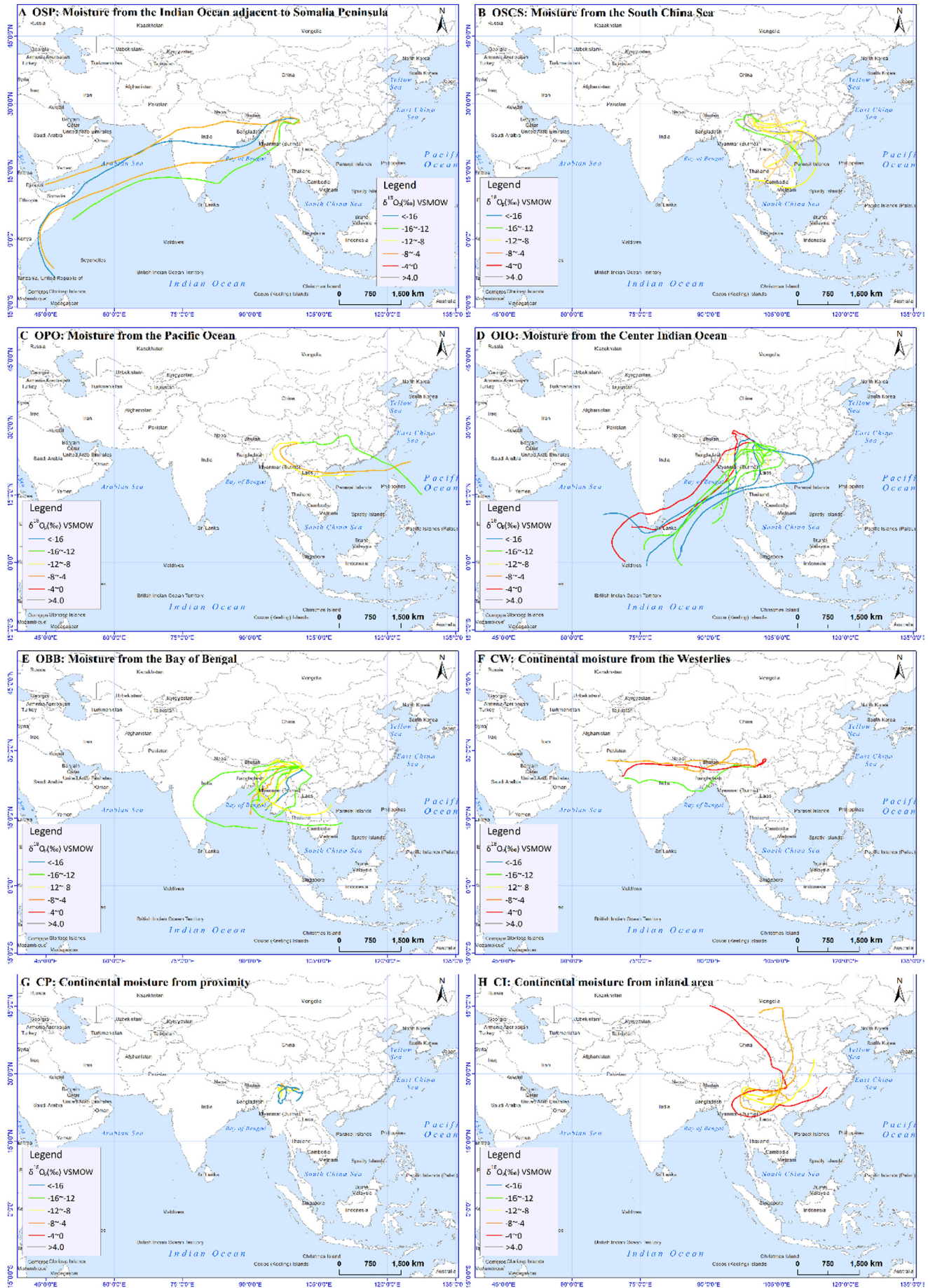


Fig. 4. Boxplot showing the distribution of $\delta^{18}\text{O}_p$, $\delta^2\text{H}_p$ and $d\text{-excess}_p$ of the south (SS) and the north precipitation (NS) of daily-based datasets in P2 (a-c), P4 (d-f), P5 (g-i) and the whole P1-P5 period (j-l).



subgroups, continent-originating (C) moisture were divided into 3 subgroups.

Moisture from the Indian Ocean adjacent to Somalia Peninsula (OSP) – Moisture originated the furthest southwest from the Indian Ocean adjacent to Somalia Peninsula, passing through the Arabian Sea and Indian inland and reaching Southwest China with a long transporting path (5768 km, Fig. 5A). Three rainfall events related to this OSP moisture and accounted for 8.1% precipitation during July and September. The isotopic composition in related rainwater had a wide range, the average $\delta^{18}\text{O}_p$ and $d\text{-excess}_p$ value of OSP were -9.7% and 1.0% , respectively.

Moisture from the South China Sea (OSCS) – The evaporated vapor water came from the South China Sea within the S-curve shape air mass trajectories having an averaged distance of 2752 km in 168 h (Fig. 5B). Eight rainfall events attributing to OSCS moisture brought 11.7% of precipitation; two-thirds of which occurred in late August and early September. The OSCS related precipitation had an average $\delta^{18}\text{O}_p$ and $d\text{-excess}_p$ value of -7.3% and 7.4% , respectively. Among the stable isotope values of OSCS, the most positive $\delta^{18}\text{O}_p$ and $d\text{-excess}_p$ value of 0.6% and 16.6% occurred on August 9.

Moisture from the Pacific Ocean (OPO) – A category having moisture sourced from the Pacific Ocean within a medium transporting pathway of 3398 km (Fig. 5C). Three precipitation events attributed to OPO moisture contributed 5.1% of rainfall. The mean $\delta^{18}\text{O}_p$ and $d\text{-excess}_p$ values of the three precipitation were -7.9% and 2.6% .

Moisture from the Center Indian Ocean (OIO) – the Indian Ocean provided vapor for eleven precipitation events, with air parcel transport over the Bay of Bengal; traveling a mean distance of 4087 km (Fig. 5D). OIO moisture belonged rainfall events accounted for 18.0% of precipitation mainly occurred in July, August and September. Precipitation related to OIO characterized the lowest average $\delta^{18}\text{O}_p$ value (-13.4%), with the second highest $d\text{-excess}_p$ values of 8.8% among all the categories. The most depleted isotope value ($\delta^{18}\text{O}_p$: -21.1%) in precipitation was collected on 7 August which decreased the average $\delta^{18}\text{O}_p$ value for this category.

Moisture from the Bay of Bengal (OBB) – Vapor fueling 25.2% of summer and fall (June, July, September and October) precipitation came from the Bay of Bengal, with air parcel transported a mean distance of 2248 km (Fig. 5E). OBB is the most frequent moisture source with 12 precipitation events in total, within almost 70% of events that happened in June, July and October. The precipitation belonging to OBB had the relatively low average $\delta^{18}\text{O}_p$ value of -12.1% and a medium averaged $d\text{-excess}_p$ value of 8.5% .

Continental moisture from the Westerlies (CW) – A branch of the westerly trajectories influencing by the Westerlies originated from the Arabian Sea, passing through Indian inland and the south of Tibetan plateau to reach Southwest China. In associated with the atmospheric circulation, four precipitation events bringing 9.3% of precipitation transported horizontally within a distance of 3323 km (Fig. 5F). CW featured a high average $\delta^{18}\text{O}_p$ value of -7.2% and the lowest averaged $d\text{-excess}_p$ value of 2.3% .

Continental moisture from proximity (CP) – A category of air mass transporting from the adjacent evaporated moisture (evaporation from surface lands and/or plant transpiration) in the shortest path (1009 km, Fig. 5G). Four precipitation events involving in CP group brought 11.7% of precipitation, characterized by the second lowest average $\delta^{18}\text{O}_p$ value of -12.6% . The average $d\text{-excess}_p$ associated with CP was 11.5% , showed the highest value among subgroups.

Continental moisture from inland area (CI) – Vapor source regions for summer precipitation were the most northerly, typically northwest China, Mongolia and central China, traveling anticlockwise around precipitation site with a moderate transporting path (2646 km; Fig. 5H). Seven precipitation events associated with CI, responsible for 11.0% of precipitation, happened in August and September. CI featured the

most enrich heavy stable isotope values (the average $\delta^{18}\text{O}_p$ value of -6.1%) and medium averaged $d\text{-excess}_p$ value of 7.9% .

4. Discussion

4.1. The impact of moisture sources on rainfall isotopic values

Multiple complex moistures contributed to local rainfall events in Southwest China (Li et al., 2017a). Among all moisture sources, ocean-originating water vapor (OBB, OIO and OSCS) contributed the most (55%) to the precipitation during the wet season. Far continental moisture (CI and CW) played the secondary role (20.3%), bringing ^{18}O (^2H)-enriched air masses. Moisture from local circulation (CP) accounted for 11.7% of precipitation, in line with the ratios of 12–34% for Hani Terrace in the southeastern section of Yunnan province (Jiao et al., 2020).

Significant discrepancies of $\delta^{18}\text{O}_p$ (ANOVA, $p = 0.016$) and $\delta^2\text{H}_p$ (ANOVA, $p = 0.012$) corresponding to their stimulated air masses sources were observed, but no significant variation was observed for $d\text{-excess}_p$ (ANOVA, $p = 0.33$) (Fig. 6). Therefore, moisture sources might have the primary effects on temporal variations of the stable isotopes in precipitation for our site. This source-specific precipitation isotope signal may attribute to the isotopic differences in vapor sources. The average $\delta^{18}\text{O}_{\text{vapor}}$ of Indian Ocean was about 6% depleted than that of the Pacific Ocean-derived moisture (Wei et al., 2018). Accordingly, the $\delta^{18}\text{O}_p$ of OIO-sourced and OBB-sourced precipitation was 5.5% lower than that of OPO-sourced and OSCS-sourced precipitation for our sites. In addition, the longer transport distance of OIO allowed for enhanced Rayleigh distillation, hence led to isotopic depletion in precipitable water compared with rainwater originating from OBB (-13.4% vs. -12.1% for $\delta^{18}\text{O}_p$) (Hoffmann et al., 2000). As illustrated above, both ocean sources and rainout effect along moisture transportation can alter the precipitation isotope ratios in Southwest China.

High temperature and relative humidity over the ocean can result in a large $d\text{-excess}$ than that of the air mass produced inland (CW and CI, Fig. 6) (Li et al., 2017b; Worden et al., 2007). The trajectories of CI evolved clockwise-rotation accompanying enriched $\delta^{18}\text{O}_p$ and medium $d\text{-excess}_p$ likely from continental Asia, such as northwest China, Mongolia Plateau and central China. The continental Asia reported $\delta^{18}\text{O}_p$ values ranged from -7.0% to -4.0% in northwest China, -12.3% to -16.4% over eastern Mongolia, -7.1% to -6.5% in central China during the warm season (Sun et al., 2020; Wang et al., 2019; Xinggang et al., 2018; Yamanaka et al., 2007). Moisture stemming from these regions mainly arose from evapotranspiration and eventually produced heavy isotope rainfall in our study area (Le Duy et al., 2018). The weighted mean $\delta^{18}\text{O}_p$ ranged from -6.5% to -5.8% , and $d\text{-excess}$ values were around 8% from July to October on the Westerlies pathway in Northern India (Juhlke et al., 2019; Sengupta and Sarkar, 2006). The slight depleted $\delta^{18}\text{O}_p$ (CW, -7.2%) in our precipitation where located at the east of Northern India might cause by rainout effect and/or other external air mass interference. Generally, the depleted isotope values of CP were more likely a mixture of lower isotope from Indian Ocean moisture with local enriched isotope recycling moisture (Jiao et al., 2020; Wang et al., 2016).

As for the depleted marine vapor of OPS, the air mass might mix with the enriched westerly vapor when it sourced from the West Indian Ocean, then passed through the Arabian Sea, Indian subcontinent and Bay of Bengal. Therefore, the rainfall $\delta^{18}\text{O}_p$ value derived from OPS was distributed between that from OIO and CW.

4.2. Regional factors on rainfall isotopic values

The temporal variation of $\delta^{18}\text{O}_p$ in the Chenghai Lake basin can be further attributed to the synchronized changes of large-scale convection

Fig. 5. Map of air mass trajectories leading up to rain events in the Chenghai Lake basin. Plots are arranged in their respective geographic moisture sources setting. Distinct colors trajectories represent different $\delta^{18}\text{O}_p$ value ranges, extend from lower than -16.0% to higher than 4.0% .

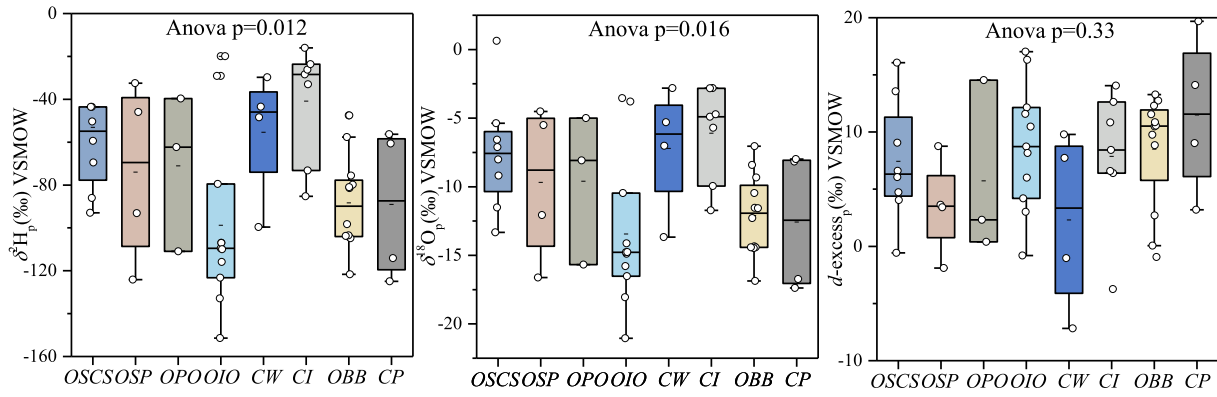


Fig. 6. The boxplot of $\delta^2\text{H}_p$, $\delta^{18}\text{O}_p$ and $d\text{-excess}_p$ data and the significant difference test based on categories of moisture sources.

activities associated with moisture sources changes (Figs. 5 and S3). During the early pre-monsoon (P1) and post-monsoon season (P4 and P5) in our study, the southern branch trough of the westerlies strengthened over the Bay of Bengal, taking the warm and humid marine airflow to the southwest China (Yu et al., 2017). The marine moisture then uplifted along the Yunnan-Guizhou Plateau where the temperature was lower and lead to abnormally high precipitation in P1 and P4 periods within depleted isotope ratios.

Westerlies trough shallowed and northward convective activities strengthened in P2 (Fig. S4). The warm and humid marine airflow from the Bay of Bengal was transported to Chenghai Lake basin, which caused increasing relative humidity and air temperature (Fig. S5). During the initial stage of Indian monsoon evolution in early June, the $\delta^{18}\text{O}_p$ was relatively high corresponded with low precipitation amounts. Coupled with the intense convection (OLR values $<200 \text{ W/m}^2$) northward to 30° N in July, the moisture from far Indian Ocean (OPS and OIO) and the Bay of Bengal (OBB) significantly increased the relative humidity and precipitation amount. The depleted vapor sourced from OPS, OIO and OBB transported a long distance to the precipitation site accompanied with continuous rainout processes, which resulted in successive depleted $\delta^{18}\text{O}_p$ precipitation.

The rainless and dry climate period of P3 could be a result of the predominance of the dry and hot northerly continental air mass. In P4 and P5, the lowest OLR value occurred at both Indian Ocean and West Pacific Ocean induced the increased moisture contribution from OSCS and OPO (Figs. S3 and S4). Within the intense convection moved toward the low-latitude, the monsoon withdrew. During the monsoon weak period (September and October, Fig. S3), the moisture was mainly controlled by the local moisture circulation, north continental wind, northern branch of the westerlies and marine air mass from OSCS and OBB. The control of dynamics in large-scale atmospheric circulation on temporal variations of precipitation stable isotopes in the Chenghai Lake basin had also been observed in other parts of southwest China, such as southern Tibetan Plateau (Yu et al., 2016; Yu et al., 2017; He and Richards, 2016), Kunming (Li et al., 2017a), Hani Terrace (Jiao et al., 2020), but with a time delay in occurrence.

The intensive convection (low OLR value) in upwind regions, especially in the Bay of Bengal, played an important role in monthly precipitation isotope ratios at the north site ($R^2 = -0.96, p < 0.01$, Table 2) but not significant for the south site.

4.3. Meteorological factors affecting isotopic characteristics

In light of the time-varying isotope values at the local spatial scale described above, we investigated the underlying links between lake-basin rainfall isotopes and local meteorological conditions at daily and monthly scale. Pearson correlation coefficients between the isotopic values and meteorological variables including precipitation amounts

(P), air temperature (T), and relative humidity (RH) were listed in Table 2.

Both $\delta^{18}\text{O}_p$ and $\delta^2\text{H}_p$ in all samples (AS) and south rainfall samples (SS) exhibited significant inverse relationships with daily local precipitation amounts. The amount effect implied that the lighter rainfall with smaller raindrops was more prone to kinetic fractionation would enrich heavy isotope ratios in the falling process (Chen et al., 2015; Yu et al., 2016). Additionally, $\delta^{18}\text{O}_p$ and $d\text{-excess}_p$ had a strong inverse correlation ($R^2 = -0.56, p < 0.01, n = 93$), suggesting that the substantial evaporation during raindrop falling drove the rainfall amount effect.

The daily air temperature rather than relative humidity was well in phase with $\delta^2\text{H}_p$ and $\delta^{18}\text{O}_p$ in AS and SS. This “anti-temperature effect” may indicate the effect of sub-cloud evaporation on precipitation stable isotopes in the wet season that was also demonstrated by previously reported results in South Asia, e.g. southwest China, Nepal (Li et al., 2017a). However, no significant correlations were found between $\delta^{18}\text{O}_p$ and meteorological factors (i.e. T, P and RH) for NS, emphasizing the different prevailing water cycle processes control on precipitation isotope ratios in SS and NS.

Table 2

Pearson correlations of isotope composition to local meteorological factors and regional climate factors (OLR) at identified primary ocean moisture sourced regions (OIO, OBB and OSCS regions) on daily-to-monthly timescale. * and ** indicate the significant level of <0.05 and <0.01 , separately.

| | | RH | T | P | OLR | | |
|---------|-------------------------|-------|--------|---------|--------|---------|-------|
| | | | | | OIO | OBB | OSCS |
| Daily | | | | | | | |
| AS | $\delta^2\text{H}_p$ | 0.03 | -0.21* | -0.26* | 0.07 | 0.18 | 0.12 |
| | $\delta^{18}\text{O}_p$ | 0.05 | -0.20 | -0.26* | 0.08 | 0.17 | 0.14 |
| | $d\text{-excess}_p$ | -0.11 | 0.03 | 0.12 | -0.13 | -0.07 | -0.17 |
| SS | $\delta^2\text{H}_p$ | 0.04 | -0.36* | -0.47** | 0.04 | 0.30 | 0.07 |
| | $\delta^{18}\text{O}_p$ | 0.06 | -0.34* | -0.45** | 0.10 | 0.27 | 0.10 |
| | $d\text{-excess}_p$ | -0.10 | 0.10 | 0.18 | -0.33* | -0.05 | -0.15 |
| NS | $\delta^2\text{H}_p$ | 0.01 | -0.12 | -0.13 | 0.12 | 0.08 | 0.13 |
| | $\delta^{18}\text{O}_p$ | 0.03 | -0.10 | -0.13 | 0.11 | 0.09 | 0.15 |
| | $d\text{-excess}_p$ | -0.13 | -0.03 | 0.06 | 0.03 | -0.09 | -0.13 |
| Monthly | | | | | | | |
| AS | $\delta^2\text{H}_p$ | -0.71 | -0.36 | -0.75 | -0.57 | 0.52 | -0.30 |
| | $\delta^{18}\text{O}_p$ | -0.46 | -0.58 | -0.66 | -0.25 | 0.76 | -0.05 |
| | $d\text{-excess}_p$ | -0.15 | 0.78 | 0.26 | -0.42 | -0.92* | -0.41 |
| SS | $\delta^2\text{H}_p$ | 0.23 | -0.71 | -0.18 | 0.57 | 0.78 | 0.82 |
| | $\delta^{18}\text{O}_p$ | 0.20 | -0.73 | -0.21 | 0.55 | 0.81 | 0.79 |
| | $d\text{-excess}_p$ | -0.05 | 0.83 | 0.36 | -0.41 | -0.89* | -0.60 |
| NS | $\delta^2\text{H}_p$ | 0.06 | 0.87 | 0.75 | -0.26 | -0.96** | -0.43 |
| | $\delta^{18}\text{O}_p$ | 0.09 | 0.87 | 0.77 | -0.24 | -0.96** | -0.43 |
| | $d\text{-excess}_p$ | -0.36 | -0.80 | -0.88* | -0.02 | 0.87 | 0.32 |

4.4. Contribution of recycled moisture or/and sub-cloud evaporation

Contrary to our hypothesis that there would be no significant difference in $\delta^2\text{H}_p$ and $\delta^{18}\text{O}_p$ values for NS and SS, the precipitation isotope values in NS was higher than in SS. The distinct relationships between isotopic values with local climate factors for NS and SS further implied that the different fractionation processes were involved in modifying the precipitation isotope signals for the two sites. Here we discussed the possible local drivers which lead to isotopic distinction for the two sites.

One possible explanation was that a contribution of recycled moisture from evaporation and transpiration in the basin caused the isotope enrichment in precipitation together with high d -excess_p at downwind site NS (Bowen et al., 2019; Corcoran et al., 2019). We assume that the moisture lead to precipitation at NS was a mixture of advection and local recycled moisture. Soil transpiration and plant evapotranspiration were not taken into account for recycling fraction estimation here, due to the massive contribution of lake evaporation (Wang et al., 2020b) and a lack of their isotope signatures during the observation period. The water vapor recycling fractions can be calculated by the following equations based on two-component isotopic mixing model:

$$\delta_p = \delta_r F_r + \delta_{adv} F_{adv} \quad (1)$$

$$F_r + F_{adv} = 1 \quad (2)$$

where δ_p , δ_r and δ_{adv} were stable isotope compositions in precipitation, lake surface evaporation vapor and advection, respectively; F_r and F_{adv} were the contribution fractions of lake evaporation vapor and advection to downwind precipitation (NS), respectively. The detailed method can be seen in Wang et al. (2016) and Zhu et al. (2019). The estimated contribution of recycled moisture (F_r) to the rainfall at downwind site NS was 7% assuming that no fractionation process occurred at upwind site SS. This result was similar with the average contribution from land surface evaporation of 5.9% in northwestern (Peng et al., 2020), 6%–18% in eastern China (Wang et al., 2016), but lower than that in eastern China Loess Plateau (28%) (Sun et al., 2020). On account of the limit meteorological strength effected on downwind $\delta^{18}\text{O}_p$ (Table 2) and restrained evaporation under high relative humidity (87.5%) during the wet season (Fig. 2), the estimated evaporation proportion seemed to be overestimated.

Another potential assumption was that a high degree of sub-cloud evaporation enriched heavy isotopes with increased d -excess_p in precipitation for NS. Precipitation at NS was more prone to sub-cloud evaporation when the southwest air masses traveled across a high altitude mountain to low surface (Fig. 1), whereas the precipitation (SS) at a higher altitude directly received atmospheric vapor replenishment. The sub-cloud evaporation calculation requires parameters such as air and dew point temperatures, evaporation rate, raindrop size and fall time of drop that were hard to evaluate precisely; instead, we used a modified method to semi-quantitatively estimate the effect of raindrop evaporation at NS compared with SS (E_f) (Froehlich et al., 2008; Peng et al., 2010):

$$E_f(\%) = (d - d_{iw}) / (-1.1(\%)) \quad (3)$$

where d and d_{iw} were the d -excess values at the sampling site (NS) and the moisture of air mass (SS). If we assumed that d_{iw} was the d -excess_p in SS, the mean calculated sub-evaporation ratio was 1.03% (E_f) higher for the downwind precipitation (NS) than at SS. This value is underestimated as we assumed that no sub-cloud evaporation occurred at SS, and it is indeed much lower than previous results obtained for e.g. Taiwan (E_f : 7–15%), northwest China (E_f : 8.3%) and eastern China Loess Plateau (E_f : 12.1%) (Chen et al., 2015; Peng et al., 2010; Sun et al., 2020).

4.5. Limitations and prospects

Although this study provides support for the coherent mechanisms for precipitation isotopic variability temporally and spatially, we

acknowledge that uncertainties and limitations exist and encourage us to continue with associated work. The analyzed meteorological data was acquired from GDAS 1 spatial $1^\circ \times 1^\circ$ dataset which might be not completely consistent with reality. Therefore, associated accurate meteorological data records from a rain gauge, weather radars (Kuriqi, 2016), etc. are needed for further studies. Besides, our one-year isotope dataset limits our ability to assess the event to annual variability of precipitation isotope which would be more solid for climate-hydrologic interpretation. Hence, long-term precipitation isotopic data collection will be expected. More long-term precipitation isotope records in other plateau lakes, such as Dianchi, Erhai, etc. will help to decipher the regional dynamics of precipitation isotopes.

In addition, our hypothesis that either recycled moisture or sub-cloud evaporation can lead to different spatial precipitation isotope patterns suggested that micro-landform and micro-climate could exert extra influence on precipitation isotopic values. To better interpret the relation between hydro-climate and precipitation $\delta^{18}\text{O}_p$, the localized isotopic changes induced by micro-topography should be get more attention.

5. Conclusions

This study investigated the drivers of the temporal and spatial change of precipitation isotope composition, and threw light on the climate-hydrological isotope construction. The regional convection activities and moisture recycling drove temporal isotopic variations, and sub-cloud evaporation or recycled moisture controlled the spatial pattern during the wet season in the Chenghai Lake basin, Southwest China. Marine moisture contributed to 68% of local precipitation and moisture from the Indian Ocean (including OIO, OBB and OSP) was the predominant contributor. The minimum $\delta^{18}\text{O}_p$ during the monsoon season was associated with strong convective activity, and the rainout effect depleted the isotope composition along the moisture transporting pathway. Whereas the increased $\delta^{18}\text{O}_p$ trend corresponded to the convection southward retreat and dominance of westerlies, north wind, local circulation and South China Sea air mass during post-monsoon season.

At daily scale, the $\delta^{18}\text{O}_p$ -precipitation amount relationship was strong, whereas $\delta^{18}\text{O}_p$ -temperature relationship was relatively weak. Additionally, 1.03% of lower sub-cloud evaporation depleted out rainfall isotope composition or 7% of recycled moisture enriched north rainfall isotope composition was individually assumed to explain the south-to-north isotope difference. More robust conclusions could be obtained with a larger set of samples. Further work for at least 48 months (Putman et al., 2019) continuous isotopic precipitation records in the Chenghai Lake basin is encouraged.

CRedit authorship contribution statement

Yajun Wang: Conceptualization, Methodology, Writing - original draft. **Yu Tang:** Writing - review & editing, Conceptualization. **Yan Xu:** Software. **Hongwei Yu:** Investigation. **Xiaofeng Cao:** Writing - review & editing. **Gaoqi Duan:** Visualization. **Lijiao Bi:** Resources. **Jianfeng Peng:** Supervision, Conceptualization.

Declaration of competing interest

There are no conflicts of interest to declare.

Acknowledgement

This research was financially supported by the Project entitled "Integrated Planning for Aquatic Eco-environmental Management in Chenghai Lake (No. 20182100702)". We also thank the NOAA Air Resources Laboratory for providing the HYSPLIT model. The list of abbreviations (Table S1) provided in the Supplementary material.

Appendix A. Supplementary data

Supplementary data to this article can be found online at <https://doi.org/10.1016/j.scitotenv.2020.143043>.

References

- Adhikari, N., Gao, J., Yao, T., Yang, Y., Dai, D., 2020. The main controls of the precipitation stable isotopes at Kathmandu, Nepal. *Tellus B: Chemical and Physical Meteorology* 72 (1), 1–17.
- Adrian, R., O'Reilly, C.M., Zagarese, H., Baines, S.B., Hessen, D.O., Keller, W., Livingstone, D.M., Sommaruga, R., Straile, D., Van Donk, E., Weyhenmeyer, G.A., Winder, M., 2009. Lakes as sentinels of climate change. *Limnol. Oceanogr.* 54 (6part2), 2283–2297.
- Bowen, G.J., Cai, Z., Fiorella, R.P., Putman, A.L., 2019. Isotopes in the water cycle: regional to global-scale patterns and applications. *Annu. Rev. Earth Planet. Sci.* 47 (1), 453–479.
- Cai, Z., Tian, L., Bowen, G.J., 2017. ENSO variability reflected in precipitation oxygen isotopes across the Asian Summer Monsoon region. *Earth Planet. Sci. Lett.* 475, 25–33.
- Cai, Z., Tian, L., Bowen, G.J., 2018. Spatial-seasonal patterns reveal large-scale atmospheric controls on Asian monsoon precipitation water isotope ratios. *Earth Planet. Sci. Lett.* 503, 158–169.
- Cai, Z., Tian, L., Bowen, G.J., 2019. Influence of recent climate shifts on the relationship between ENSO and Asian Monsoon precipitation oxygen isotope ratios. *J. Geophys. Res.-Atmos.* 124, 7825–7835.
- Cao, X., Xu, X., Bian, R., Wang, Y., Yu, H., Xu, Y., Duan, G., Bi, L., Chen, P., Gao, S., Wang, J., Peng, J., Qu, J., 2020. Sedimentary ancient DNA metabarcoding delineates the contrastingly temporal change of lake cyanobacterial communities. *Water Res.* 183, 116077.
- Chen, F., Zhang, M., Wang, S., Ma, Q., Zhu, X., Dong, L., 2015. Relationship between sub-cloud secondary evaporation and stable isotopes in precipitation of Lanzhou and surrounding area. *Quat. Int.* 380–381, 68–74.
- Chen, X., Liu, X., Peng, W., Dong, F., Chen, Q., Sun, Y., Wang, R., 2019. Hydroclimatic influence on the salinity and water volume of a plateau lake in Southwest China. *Sci. Total Environ.* 659, 746–755.
- Corcoran, M.C., Thomas, E.K., Boutt, D.F., 2019. Event-based precipitation isotopes in the Laurentian Great Lakes region reveal spatiotemporal patterns in moisture recycling. *Journal of Geophysical Research: Atmospheres* 124 (10), 5463–5478.
- Craig, H., 1961. Isotopic variations in meteoric waters. *Science* 133 (3465), 1702–1703.
- Dansgaard, W.F., 1964. Stable isotopes in precipitation. *Tellus* 16, 436–468.
- Froehlich, K., Kralik, M., Papesch, W., Rank, D., Scheifinger, H., Stichler, W., 2008. Deuterium excess in precipitation of alpine regions – moisture recycling. *Isotopes in Environmental & Health Studies* 44 (1), 61–70.
- Gottfried, M., Pauli, H., Futschik, A., Akhalkatsi, M., Barančok, P., Benito Alonso, J.L., Coldea, G., Dick, J., Erschbamer, B., Fernández Calzado, M.A.R., Kazakis, G., Kraljić, J., Larsson, P., Mallaun, M., Michelsen, O., Moiseev, D., Moiseev, P., Molau, U., Merzouki, A., Nagy, L., Nakhutsrishvili, G., Pedersen, B., Pelino, G., Puscas, M., Rossi, G., Stanisci, A., Theurillat, J.-P., Tomaselli, M., Villar, L., Vittoz, P., Vogiatzakis, I., Grabherr, G., 2012. Continent-wide response of mountain vegetation to climate change. *Nat. Clim. Chang.* 2 (2), 111–115.
- Harsch, M.A., Hulme, P.E., McGlone, M.S., Duncan, R.P., 2009. Are treelines advancing? A global meta-analysis of treeline response to climate warming. *Ecol. Lett.* 12 (10), 1040–1049.
- He, S., Richards, K., 2016. Stable isotopes in monsoon precipitation and water vapour in Nagqu, Tibet, and their implications for monsoon moisture. *J. Hydrol.* 540, 615–622.
- He, S., Goodkin, N.F., Kurita, N., Wang, X., Rubin, C.M., 2018. Stable isotopes of precipitation during tropical Sumatra squalls in Singapore. *Journal of Geophysical Research: Atmospheres* 123 (7), 3812–3829.
- Hillman, A.L., Abbott, M.B., Yu, J., Steinman, B.A., Bain, D.J., 2016. The isotopic response of Lake Chenghai, SW China, to hydrologic modification from human activity. *The Holocene* 26 (6), 906–916.
- Hoffmann, G., Jouzel, J., Masson-Delmotte, V., 2000. Stable water isotopes in atmospheric general circulation models. *Hydrol. Process.* 14, 1385–1406.
- Jiao, Y., Liu, C., Liu, Z., Ding, Y., Xu, Q., 2020. Impacts of moisture sources on the temporal and spatial heterogeneity of monsoon precipitation isotopic altitude effects. *J. Hydrol.* 583, 124576.
- Juhlke, T., Meier, C., van Geldern, R., Vanselow, K., Wernicke, J., Baidulloeva, J., Barth, J. and Weise, S. (2019) Assessing moisture sources of precipitation in the Western Pamir Mountains (Tajikistan, Central Asia) using deuterium excess. *Tellus B: Chemical and Physical Meteorology* 71, 1–16.
- Kuriqi, A., 2016. Assessment and quantification of meteorological data for implementation of weather radar in mountainous regions. *Mausam* 67, 789–802.
- Le Duy, N., Heidbüchel, I., Meyer, H., Merz, B., Apel, H., 2018. What controls the stable isotope composition of precipitation in the Mekong Delta? A model-based statistical approach. *Hydrol. Earth Syst. Sci.* 22 (2), 1239–1262.
- Li, G., Zhang, X., Xu, Y., Wang, Y., Wu, H., 2017a. Synoptic time-series surveys of precipitation $\delta^{18}O$ and its relationship with moisture sources in Yunnan, Southwest China. *Quat. Int.* 440, 40–51.
- Li, Y., Rao, Z., Cao, J., Jiang, H., Gao, Y., 2017b. Highly negative oxygen isotopes in precipitation in Southwest China and their significance in paleoclimatic studies. *Quat. Int.* 440, 64–71.
- Liebmann, B., Smith, C., 1996. Description of a complete (interpolated) outgoing longwave radiation dataset. *Bull. Amer. Meteor. Soc.* 77, 1275–1277.
- MacDonald, G.M., Moser, K.A., Bloom, A.M., Potito, A.P., Porinchu, D.F., Holmquist, J.R., Hughes, J., Kremenetski, K.V., 2016. Prolonged California aridity linked to climate warming and Pacific Sea surface temperature. *Sci. Rep.* 6 (1), 33325.
- Moser, K.A., Baron, J.S., Brahney, J., Oleksy, I.A., Saros, J.E., Hundey, E.J., Sadro, S.A., Kopáček, J., Sommaruga, R., Kainz, M.J., Strecker, A.L., Chandra, S., Walters, D.M., Preston, D.L., Michelutti, N., Lepori, F., Spaulding, S.A., Christianson, K.R., Melack, J.M., Smol, J.P., 2019. Mountain lakes: eyes on global environmental change. *Glob. Planet. Chang.* 178, 77–95.
- Narancic, B., Wolfe, B.B., Pienitz, R., Meyer, H., Lamhonwah, D., 2017. Landscape-gradient assessment of thermokarst lake hydrology using water isotope tracers. *J. Hydrol.* 545, 327–338.
- Nlend, B., Celle-Jeanton, H., Risi, C., Pohl, B., Huneau, F., Ngo Boum-Nkot, S., Seze, G., Roucou, P., Camberlin, P., Etame, J., Ketchemen-Tandia, B., 2020. Identification of processes that control the stable isotope composition of rainwater in the humid tropical west-Central Africa. *J. Hydrol.* 584, 124650.
- Peng, T.-R., Wang, C.-H., Huang, C.-C., Fei, L.-Y., Chen, C.-T.A., Hwong, J.-L., 2010. Stable isotopic characteristic of Taiwan's precipitation: a case study of western Pacific monsoon region. *Earth Planet. Sci. Lett.* 289 (3–4), 357–366.
- Peng, P., Zhang, X.J., Chen, J., 2020. Modeling the contributions of oceanic moisture to summer precipitation in eastern China using 18O. *J. Hydrol.* 581, 124304.
- Putman, A., Fiorella, R., Bowen, G., Cai, Z., 2019. A global perspective on local meteoric water lines: meta-analytic insight into fundamental controls and practical constraints. *Water Resour. Res.* 55 (8), 6896–6910.
- Sadro, S., Sickman, J.O., Melack, J.M., Skeen, K., 2018. Effects of climate variability on snow-melt and implications for organic matter in a high-elevation lake. *Water Resour. Res.* 54 (7), 4563–4578.
- Sengupta, S., Sarkar, A., 2006. Stable isotope evidence of dual (Arabian Sea and Bay of Bengal) vapour sources in monsoonal precipitation over north India. *Earth Planet. Sci. Lett.* 250 (3–4), 511–521.
- Sinha, N., Chakraborty, S., 2020. Isotopic interaction and source moisture control on the isotopic composition of rainfall over the Bay of Bengal. *Atmos. Res.* 235, 104760.
- Stein, A., Draxler, R.-R., Rolph, G., Stunder, B., Cohen, M.-D., Ngan, F., 2016. NOAA's HYSPLIT atmospheric transport and dispersion modeling system. *Bull. Am. Meteorol. Soc.* 96 (12), 2059–2077.
- Sun, W., Zhang, E., Shulmeister, J., Bird, M.I., Chang, J., Shen, J., 2019. Abrupt changes in Indian summer monsoon strength during the last deglaciation and early Holocene based on stable isotope evidence from Lake Chenghai, southwest China. *Quat. Sci. Rev.* 218, 1–9.
- Sun, C., Chen, W., Chen, Y., Cai, Z., 2020. Stable isotopes of atmospheric precipitation and its environmental drivers in the eastern Chinese loess plateau, China. *J. Hydrol.* 581, 124404.
- Tang, Y., Song, X., Zhang, Y., Han, D., Ai, L., Zhao, T., Wang, Y., 2017. Using stable isotopes to understand seasonal and interannual dynamics in moisture sources and atmospheric circulation in precipitation. *Hydrol. Process.* 31 (26), 4682–4692.
- Tao, S., Fang, J., Ma, S., Cai, Q., Xiong, X., Tian, D., Zhao, X., Fang, L., Zhang, H., Zhu, J., Zhao, S., 2020. Changes in China's lakes: climate and human impacts. *Natl. Sci. Rev.* 7, 132–140.
- Walter Anthony, K., Schneider von Deimling, T., Nitze, I., Frolking, S., Emond, A., Daanen, R., Anthony, P., Lindgren, P., Jones, B., Grosse, G., 2018. 21st-century modeled permafrost carbon emissions accelerated by abrupt thaw beneath lakes. *Nat. Commun.* 9, 3262.
- Wang, S., Zhang, M., Che, Y., Chen, F., Qiang, F., 2016. Contribution of recycled moisture to precipitation in oases of arid central Asia: a stable isotope approach. *Water Resour. Res.* 52 (4), 3246–3257.
- Wang, L., Dong, Y., Han, D., Xu, Z., 2019. Stable isotopic compositions in precipitation over wet island in Central Asia. *J. Hydrol.* 573, 581–591.
- Wang, D., Tian, L., Cai, Z., Shao, L., Guo, X., Tian, R., Li, Y., Chen, Y., Yuan, C., 2020a. Indian monsoon precipitation isotopes linked with high level cloud cover at local and regional scales. *Earth Planet. Sci. Lett.* 529, 115837.
- Wang, Y., Peng, J., Cao, X., Xu, Y., Yu, H., Duan, G., Qu, J., 2020b. Isotopic and chemical evidence for nitrate sources and transformation processes in a plateau lake basin in Southwest China. *Sci. Total Environ.* 711, 134856.
- Wei, Z., Lee, X., 2019. The utility of near-surface water vapor deuterium excess as an indicator of atmospheric moisture source. *J. Hydrol.* 577, 123923.
- Wei, Z., Lee, X., Liu, Z., Seeboonruang, U., Koike, M., Yoshimura, K., 2018. Influences of large-scale convection and moisture source on monthly precipitation isotope ratios observed in Thailand, Southeast Asia. *Earth Planet. Sci. Lett.* 488, 181–192.
- Worden, J., Noone, D., Bowman, K., The Tropospheric Emission Spectrometer Science, T. and Data, c. 2007. Importance of rain evaporation and continental convection in the tropical water cycle. *Nature* 445, 528–532.
- Xinggang, M., Wenxiang, J., Guofeng, Z., Dan, D., Hanxiang, P., Xiuting, X., Huiwen, G., Yu, Z., Ruifeng, Y., 2018. Stable isotope composition of precipitation at different elevations in the monsoon marginal zone. *Quat. Int.* 493, 86–95.
- Xu, T., Sun, X., Hong, H., Wang, X., Cui, M., Lei, G., Gao, L., Liu, J., Lone, M.A., Jiang, X., 2019. Stable isotope ratios of typhoon rains in Fuzhou, Southeast China, during 2013–2017. *J. Hydrol.* 570, 445–453.
- Yamanaka, T., Tsujimura, M., Oyunbaatar, D., Davaa, G., 2007. Isotopic variation of precipitation over eastern Mongolia and its implication for the atmospheric water cycle. *J. Hydrol.* 333 (1), 21–34.
- Yu, W., Wei, F., Ma, Y., Liu, W., Zhang, Y., Luo, L., Tian, L., Xu, B., Qu, D., 2016. Stable isotope variations in precipitation over Deqin on the southeastern margin of the Tibetan Plateau during different seasons related to various meteorological factors and moisture sources. *Atmos. Res.* 170, 123–130.

- Yu, W., Tian, L., Yao, T., Xu, B., Wei, F., Ma, Y., Zhu, H., Luo, L., Qu, D., 2017. Precipitation stable isotope records from the northern Hengduan Mountains in China capture signals of the winter India–Burma Trough and the Indian Summer Monsoon. *Earth Planet. Sci. Lett.* 477, 123–133.
- Zhang, G., Yao, T., Chen, W., Zheng, G., Shum, C.K., Yang, K., Piao, S., Sheng, Y., Yi, S., Li, J., O'Reilly, C.M., Qi, S., Shen, S.S.P., Zhang, H., Jia, Y., 2019. Regional differences of lake evolution across China during 1960s–2015 and its natural and anthropogenic causes. *Remote Sens. Environ.* 221, 386–404.
- Zhu, G., Guo, H., Qin, D., Pan, H., Zhang, Y., Jia, W., Ma, X., 2019. Contribution of recycled moisture to precipitation in the monsoon marginal zone: estimate based on stable isotope data. *J. Hydrol.* 569, 423–435.